Induced Seismicity Forecasting Research Service

Technical Report

Prepared for:

UK Oil & Gas Authority

Oil & Gas Authority

Version 2.0

Date: September 23, 2019

DISCLAIMER: PLEASE READ CAREFULLY.

The information contained in this document is intended to report and provide insights for the internal use of the recipient, who accepts full responsibility for its use. Nanometrics Inc. makes no representations or warranties of any kind, express or implied about the completeness, accuracy, reliability, suitability or availability with respect to this document or the information or related graphics contained within. Without limiting the foregoing, Nanometrics Inc. specifically disclaims any responsibility if such document is inaccurate, incomplete or misleading at the time of distribution.

The findings in this document should be assessed as a whole and any attempt to rely on partial analysis or summary descriptions in this document could lead to undue emphasis on particular factors or inaccurate conclusions. This document has been provided in good faith based on data collected by Nanometrics Inc., which was available at the time that the document was generated.

In no event will Nanometrics Inc. or its partners, suppliers, employees or agents, be liable to the recipient or anyone else for any loss, damage, cost or expense of any kind, including any consequential, special or similar damages, arising in connection with results obtained from the use of this information, any decision made or action taken in reliance on this document or any information contained in this document. Any reliance you place on such material is therefore strictly at the recipient's own risk.

Table of Content

Summary

The goal of this research project is to identify where predictive tools may have been useful in providing early warning to mitigate against larger, potentially felt induced events and understanding the strengths and pitfalls of these techniques, in particular, minimum event constraints, and their predictive performance against the recorded seismicity.

During the operations at Preston New Road (PNR) in 2018, the operator ran two real-time systems to record microseismic-macroseismic data including a surface array of 8 seismometers with the purpose of Traffic Light System and a Downhole Microseismic Monitoring Array. These two datasets are played back to simulate real-time scenarios and are used to perform the following tests:

- Examine the predictive forecasting methodologies that have been integrated into the Nanometrics Seismic Management Dashboard including one model from Shapiro et al. (2010) and two models from van Der Elst et al. (2016).
- Investigate the predictive forecasting of recently published Verdon and Budge (2018) approach using the model from Hallo et al. (2014).

In this report, we test the dashboard using solely the downhole microseismic data, solely the surface microseismic data and combination of the surface and downhole data datasets from PNR hydraulic fracture (HF) operations.

Introduction

Stress changes due to subsurface fluid injection may induce seismicity. The size and distribution of such events are a function of existing geological structures and treatment parameters. Not all of the fluid injection operations exhibit seismicity (Shultz et al 2018), but when they do it is vital to monitor the on-going induced seismic activity for invoking risk mitigation plans.

The majority of the regulatory traffic light protocols introduced to date are based on staged magnitude thresholds, which increases the need for a better estimation of the largest magnitude possible event that is related to oil and gas production. Forecasting maximum magnitude in real-time is a subject of significant interest to many operators. Prior knowledge of the largest possible event in real-time allows operators to optimise and adjust their stimulation plans accordingly to prevent events that would trigger regulation-driven operational shutdowns.

A large body of work has been published on forecasting maximum magnitude (Mmax) related to fluid injection in a given area. The performance of these models has been assessed in several studies (Karimi and Baturan 2018, Eaton and Igonin 2018, Schultz et al. 2018, Kiraly-Proag et al. 2016) using available datasets to identify the benefits and challenges of each method.

Shapiro et al. (2010) introduced a parameter called 'seismogenic index' which represents the tectonic feature of a given location and is independent of injection parameters. Using this index, cumulative injected volume, and an estimated b-value, one can calculate the number of events within a specific magnitude range and consequently determine the probability of events occurring that have a magnitude larger than the threshold magnitude that results during fluid injection (referred to hereafter as SH10). The result from this method is valid during active fluid injection.

Shapiro et al. (2011) stated that the minimum principal stress axis of the fluid-stimulated rock volume is one of the main factors limiting the probability of large magnitude events. This model essentially relates the fluid-injected Mmax with geometrical characteristics of the simulated volume (i.e., the microseismic cloud). This method suggests real-time monitoring of the spatial growth of seismicity during rock stimulation to estimate expected Mmax and consequently to mitigate the seismicity risk.

250 Herzberg Road, Kanata, Ontario, Canada K2K 2A1
Tel +1 613 592 6776 | **Toll Free** 1 855 792 6776 (NA) | **Fax** +1 613 592 5929

McGarr (2014) developed a simple relationship between the cumulative volume of injected fluid and the largest seismic moment. This model is developed based on some assumptions, including a fully saturated, brittle rock mass with a b-value of 1.0.

Hallo et al. (2014) modified the model introduced by McGarr (2014) to account for aseismic slip to explain observed seismic moment. The new parameter, called 'seismic efficiency ratio', is a ratio of the released to the theoretical scalar cumulative moment. Verdon and Budge (2018) showed that adding a value of 0.5 to the new model is sufficient to capture 95% of the variance between true and reconstructed model populations (referred to hereafter as H14).

Van Der Elst et al. (2016) demonstrated that the size of the strongest events from seismic activities related to fluid injection is consistent with the sampling statistics of the Gutenberg-Richter distribution for tectonic events. They concluded that injection controls the nucleation but that earthquake magnitude is controlled by tectonic processes. They introduced a model based on this hypothesis (referred to hereafter as $VDE16_{Seis}$). They further linked their model to total injected volume and seismogenic index (referred to hereafter as $VDE16_{SI\text{-}V}$).

Eaton and Igonin (2018) added a tapered Gutenberg-Richter relationship to $VDE16_{Seis}$, to introduce a limit to the size of the maximum magnitude event.

Karimi and Baturan (2018) investigated six published methods and decided not to utilise three of them in the forecasts. Shapiro et al. (2011) do not account for the far-field triggering due to poroelastic stress effect and neglect nucleation of an event in the stimulated volume while the fault continues out of the event cloud. Their analyses show that McGarr (2014) overestimates Mmax compared to the observations. Furthermore, McGarr's model is developed based on assumptions including a constant b-value of 1. Eaton and Igonin (2018) limit the upper magnitude level in the real-time application which we did not prefer.

In this research, we investigate the predictive forecasting of SH10, VDE16Seis, VDE16SI-V and H14 at regular time intervals (e.g., Kiraly-Proag et al. 2016 and Verdon and Budge 2018) through Nanometrics Seismic Management Dashboard. A minimum of 100 events is the default requirement to start the statistical analysis. Figure 1 provides a description for each panel of the dashboard.

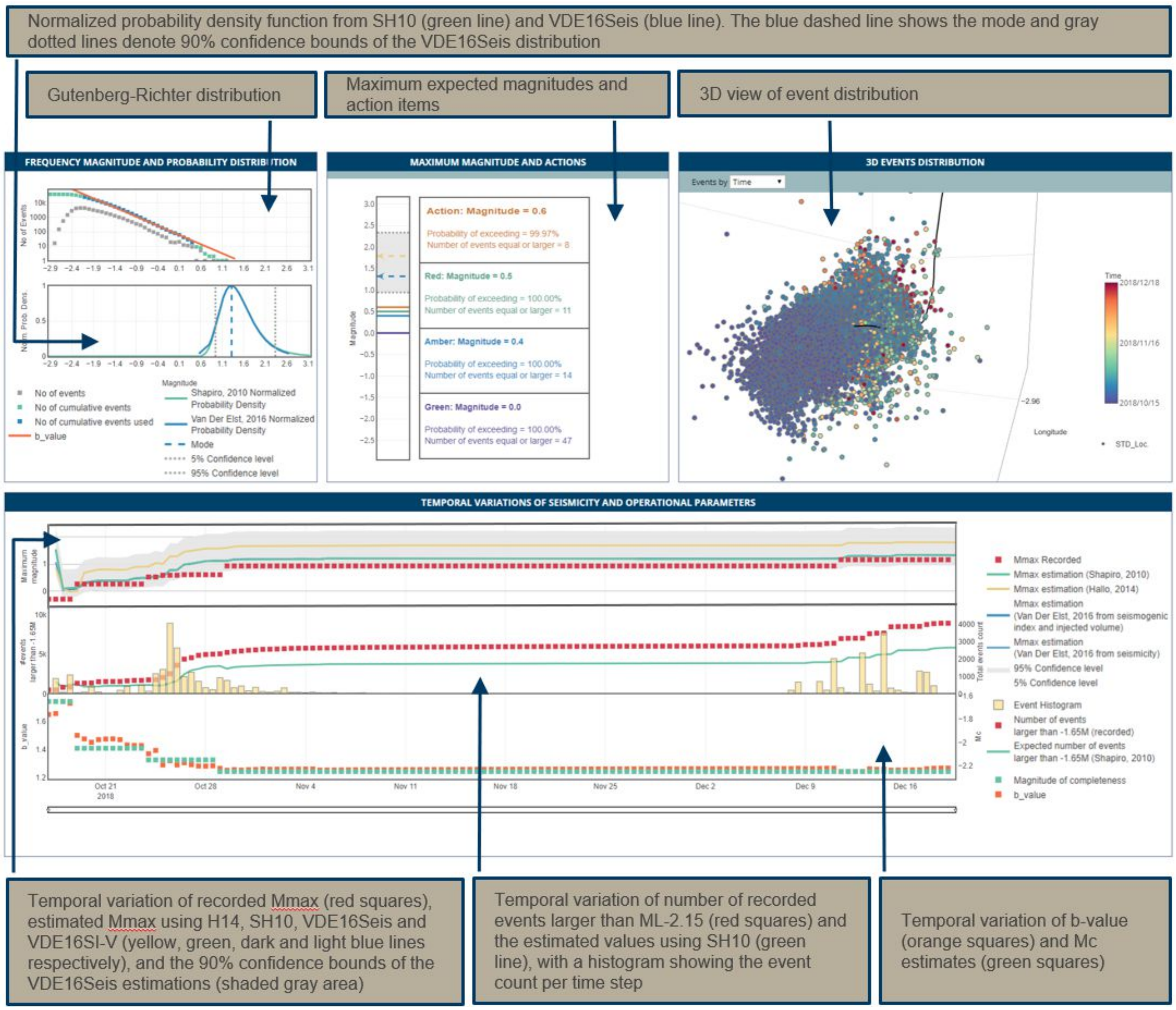

Figure 1: Example Nanometrics Seismic Management Dashboard with description of each panel

Appendix A contains all the figures presented in this report with maximum size for better visibility.

Data

Downhole catalog

The real-time downhole microseismic monitoring array consists of 12 slim-hole, 3-component, 15 Hz geophones. A total of 38,384 events have been picked, with magnitudes ranging from Mw-2.839 to Mw1.155 , where larger events have either caused clipping, saturate the low-frequency response, or both. The magnitude of completeness (Mc) estimated for this dataset, using the maximum curvature method is Mw-2.25 and the duration of recorded data is 64 days (Figure 2).

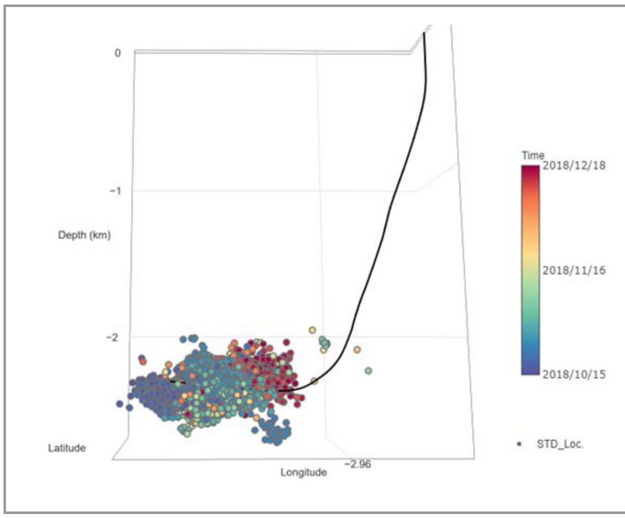

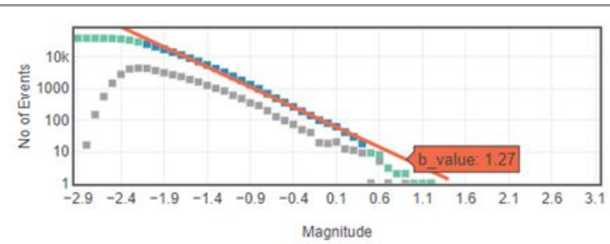

Figure 2: (Left) 3D distribution of the recorded seismicity by the downhole monitoring array (Top) Gutenberg-Richter distribution for the entire catalog with b-value of 1.27

Surface catalog

For the purpose of the Traffic Light System, a surface array of 8 real-time sensors, including 2 broadband seismometers and 6 4.5 Hz geophones were deployed. In total 57 events were detected during operations, with a minimum detection threshold of ML-0.8, a magnitude of completeness of ML-0.05, and the maximum event recorded of ML1.5. The duration of recorded data for this data set is 57 days (Figure 3).

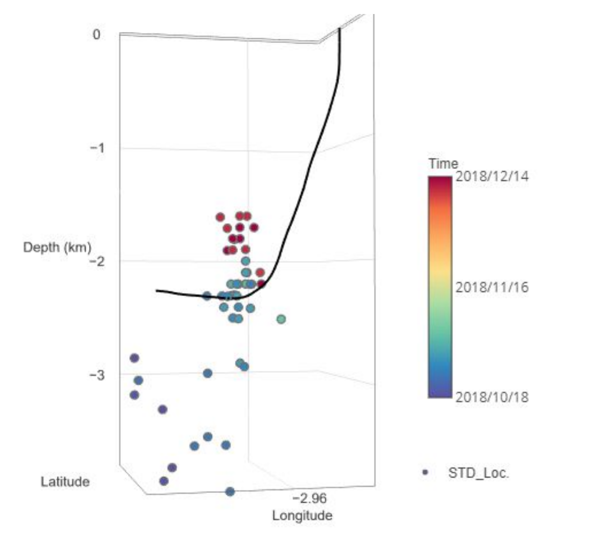

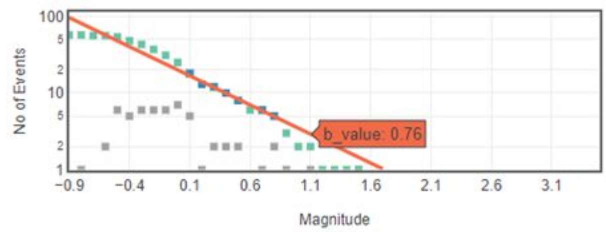

Figure 3: (Left) 3D distribution of the recorded seismicity by the surface array (Top) Gutenberg-Richter distribution for the entire catalog with b-value of 0.76

Testing the forecasting models

To simulate real-time monitoring, we played back the data and calculated the b-value and Mc at regular time intervals from the cumulative seismicity data. In addition to seismicity parameters at each time interval, we also estimated the 'seismogenic index' and 'seismic efficiency ratio'. We used these parameters to estimate the expected maximum magnitude (Mmax) and the number of events that exceed a threshold magnitude at each time step and compared them to the recorded seismicity.

Impact of cumulative injection volume on the forecasts

Karimi and Baturan (2018) showed that cumulative injection volume has little to no impact on forecasted seismicity, and over time, forecast lose their sensitivity to the cumulative injection volume. Following Kiraly-Proag et al. (2016) and Verdon and Budge (2018), we reevaluate b-value, Mc, seismogenic index and seismic efficiency at every time step taking into account the cumulative injection volume and the cumulative recorded seismicity from the current time. Then these parameters and the designed cumulative injection volume data from the next time step are used to forecast the seismicity. The relationship between Mmax and cumulative volume is in the form of equation 1:

$$Mmax \sim log \frac{Cumulative\ Volume2}{Cumulative\ Volume1} \qquad (1)$$

Where Cumulative Volume 1 is the cumulative injection volume at current time and Cumulative Volume 2 is the cumulative injection volume at the next time step.

As cumulative injection volume grows in time, the logarithm of the ratio of current cumulative injection volume to the cumulative injection volume at the next time step decreases, and as a result, the Mmax estimation is not very sensitive to changes in the total injection volume.

To test the impact of cumulative volume data on the estimated seismicity, we reevaluate all parameters with and without considering the real cumulative injection volume using the catalog recorded by the downhole array during stimulation of sleeve 38, where the largest event with the magnitude of Mw1.15 occurred. As mentioned before this magnitude is likely underestimated due to clipping. Figure 4 presents the observations and forecasts over time when we include the real cumulative injection volume. Figure 5 shows the forecast values using a constant injection rate. A comparison of the estimated maximum magnitudes and the number of events from Figure 4 and Figure 5 demonstrates the limited impact that injection volume data has on the forecasts. As an example the final forecasting Mmax from $VDE16_{Seis}$ model using real and simulated injection volume data is Mw0.91

Following this conclusion, for the tests, real cumulative injection volume was replaced by a simulated cumulative injection volume with a steadily increasing rate. The independence of forecasts from treatment data assists with the operational functionality of the dashboard in real-time operational use cases.

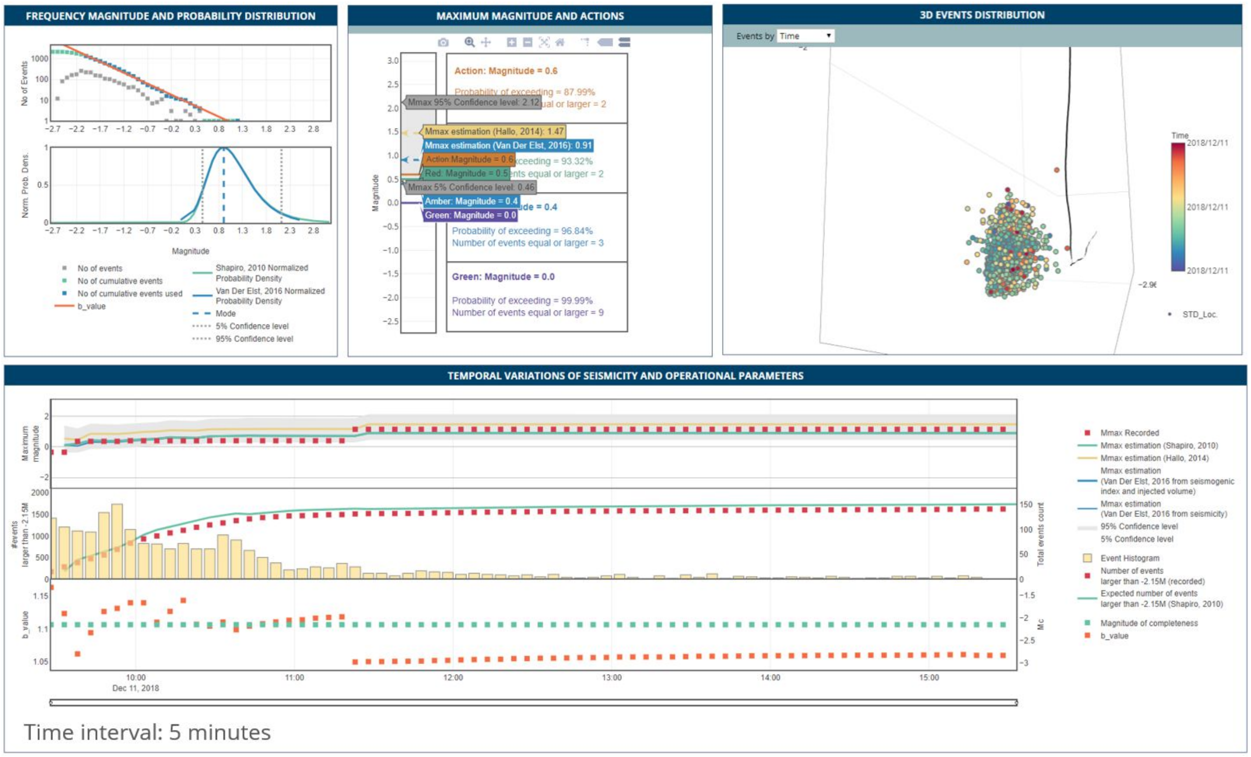

Figure 4: Dashboard for recorded seismicity by the downhole array during stimulation on sleeve 38 using real cumulative injection volume

Figure 5: Dashboard for recorded seismicity by the downhole array during stimulation of sleeve 38 using simulated cumulative injection volume with a steady increasing rate (see the caption of Figure 1 for descriptions of each panel)

Downhole data

Stages with events larger than Mw0.5

We run the dashboard with a five minutes time interval for the recorded seismicity during seven stages with recorded events larger than Mw0.5 including:

Sleeve 14, with observed Mmax of Mw0.52

Our analysis shows that for most of the stages, the models successfully forecast the Mmax, However, this is not always the case, as highlighted in Figure 6 for stage 14 where the largest event occurred early in the sequence before recording the minimum 100 events to start the statistical analysis (recorded Mmax in red squares and estimated Mmax using H14, SH10, VDE16Seis and VDE16SI-V in yellow, green, dark and light blue lines respectively).

Figure 6: Dashboard for recorded seismicity by the downhole array during stimulation of sleeve 14, with observed Mmax of Mw0.52 (see the caption of Figure 1 for descriptions of each panel)

Sleeve 18, with observed Mmax of Mw0.59

Playing back the data recorded during sleeve 18 shows that in the real-time application the dashboard would provide 10 minutes notice of a large event (highlighted by the red box in Figure 7). The forecasting models and the Gutenberg-Richter distribution exhibit the expectation of a larger event by the end of this stage (Figure 7).

Figure 7: Dashboard for recorded seismicity by the downhole array during stimulation of sleeve 18, with observed Mmax of Mw0.59 (see the caption of Figure 1 for descriptions of each panel)

Sleeve 30, with observed Mmax of Mw0.61

The analysis of stage 30 indicates a substantial rise in the number and size of events over less than an hour. Although the H14 model (yellow line) predicted rising magnitude ~25 minutes prior to the Mw0.61 event, in general, it overestimates the magnitude during the stimulation time. The expected number of events from the SH10 model (green line) agrees well with the observations (Figure 8).

Figure 8: Dashboard for recorded seismicity by the downhole array during stimulation of sleeve 30, with observed Mmax of Mw0.61 (see the caption of Figure 1 for descriptions of each panel)

Sleeve 31, with observed Mmax of Mw0.61

The largest event from stage 31 with the magnitude of Mw0.61 occurred early during stimulation. SH10, $VDE16_{Seis}$ and $VDE_{16SI\text{-}V}$ models did not forecast this event. Although the H14 model provides 5 minutes notice, again, in general, this model overestimates Mmax (Figure 9).

Figure 9: Dashboard for recorded seismicity by the downhole array during stimulation of sleeve 31 with observed Mmax of Mw0.61 (see the caption of Figure 1 for descriptions of each panel)

Sleeve 32, with observed Mmax of Mw0.93

Figure 10 illustrates the results from playing back the seismic catalog recorded during stage 32 stimulation. Although all forecasting models expected a large event ~8 hours prior to the event with a magnitude of Mw0.93, they all underpredicted the Mmax.

Figure 10: Dashboard for recorded seismicity by the downhole array during stimulation of sleeve 32, with observed Mmax of Mw0.93 (see the caption of Figure 1 for descriptions of each panel)

Sleeve 35, with observed Mmax of Mw0.59

The maximum magnitude recorded during stage 35 stimulation was Mw0.59. H14 (yellow line) model forecasted this event 41 hours earlier. As shown in the top left panel of Figure 11, this event is well above the expectation from the GR distribution.

Figure 11: Dashboard for recorded seismicity by the downhole array during stimulation of sleeve 35, with observed Mmax of Mw0.59 (see the caption of Figure 1 for descriptions of each panel)

Sleeve 38, with observed Mmax of Mw1.15

The largest event recorded during the operation occurred during the stimulation of stage 38. The 15 Hz downhole geophones clipped and reported the magnitude as Mw1.15. The surface catalog listed this event as ML1.5. H14 model forested this event ~80 minutes earlier (Figure 12). The result from the SH10 model for the number of events is in very good agreement with the observations, as well.

Figure 12: Dashboard for recorded seismicity by the downhole array during stimulation of sleeve 38, with observed Mmax of Mw1.15 (see the caption of Figure 1 for descriptions of each panel)

The results from the stage-by-stage analysis show that the predictive models were not very successful in forecasting maximum magnitude. While the large events in most cases are forecasted by Hallo et al. 2014 model, this model overestimated the maximum magnitude in general. Our findings show that the notification time for many successful forecasts is very short which would not be sufficient enough to perform practical operational actions.

Entire downhole catalog

During the operation, injecting each stage would change the stress condition. By focusing on individual stages, the overall changes in the stress field would be ignored and as a result, the forecasting models would not be very successful to capture the current stress condition. In this section, we demonstrate that using the complete catalog, improves the forecasting outcome.

We performed statistical analysis using the entire recorded downhole catalog. As shown in Figure 13 there are 4 major increasing steps in the size of events over the time of monitoring. Although generally, Hallo et al 2014 (yellow line) model overestimated the maximum magnitude, the prediction models successfully forecasted all 4 events with advance notification varying between 1 to 16 days. The outcomes from this exercise confirm that using the entire catalog improved forecasting with an earlier notification time.

Surface data

Along with the downhole system, the operation was monitored by a surface network consisting of 8 real-time sensors, including 2 broadband seismometers and 6 4.5 Hz geophones. Although the total number of recorded events by this network is 57 and fewer than our proposed minimum required number of events (100), we played back the data and investigated the predictions of the forecasting models with 24 hours time interval. We do not recommend this in real-time applications.

The result from the statistical analysis shows all forecasting models successfully predicted the largest event with a magnitude of ML1.5 with ~44 days notification time (Figure 14).

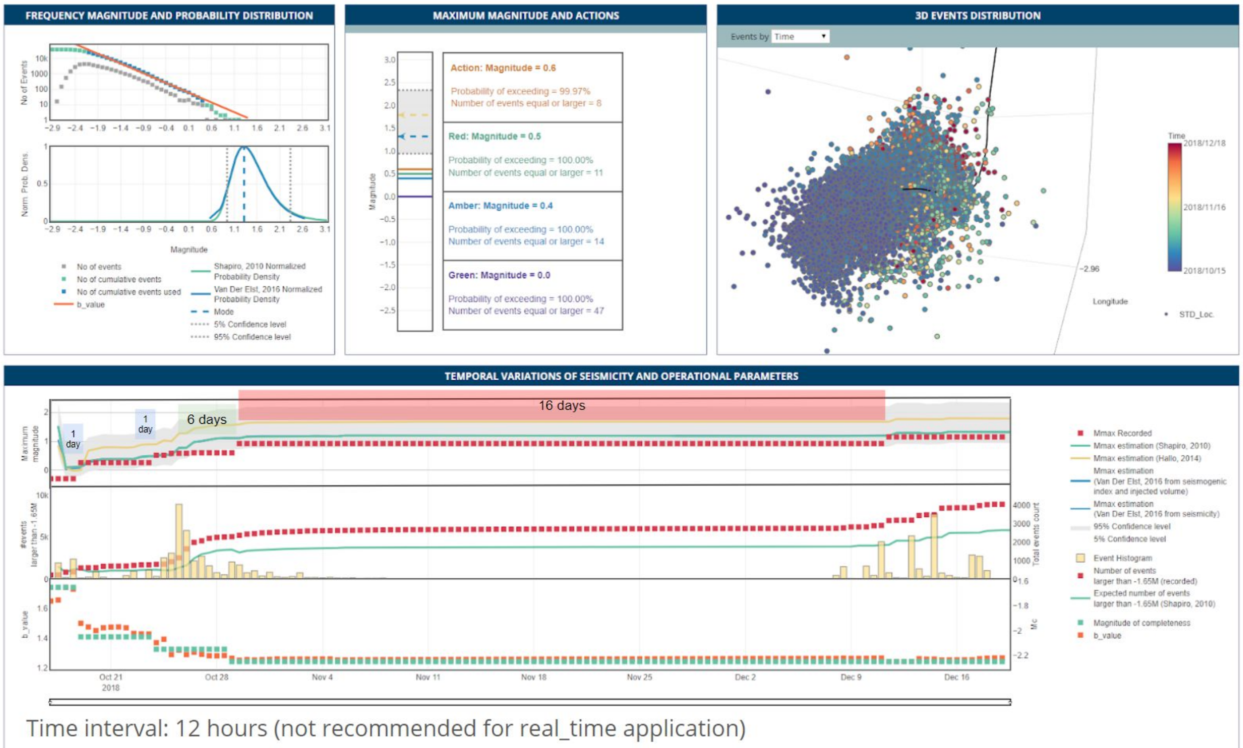

Figure 13: Dashboard for the entire recorded seismicity by the downhole array. The forecasting notification time is highlighted. (see the caption of Figure 1 for descriptions of each panel)

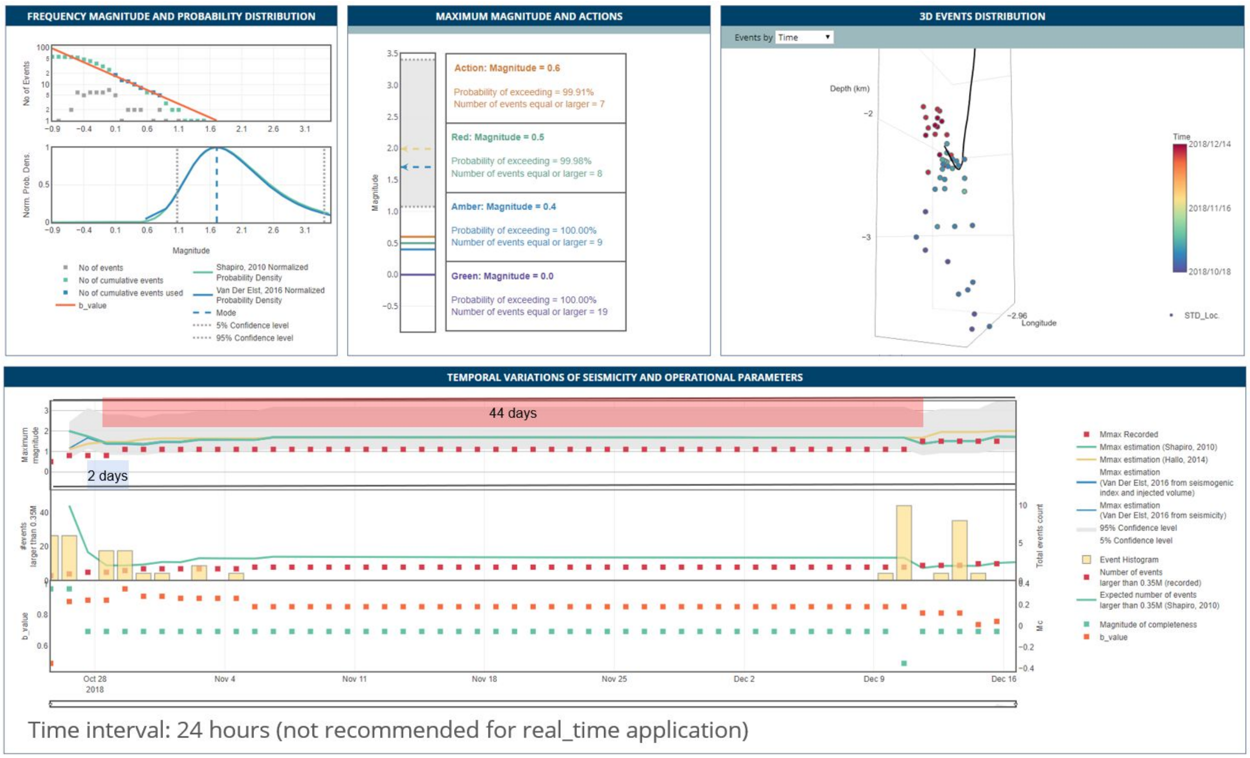

Figure 14: Dashboard for the entire recorded seismicity by the surface array (see the caption of Figure 1 for descriptions of each panel)

Figure 15 illustrates the Gutenberg-Richter distribution before and after the largest event with magnitude ML1.5. As it is illustrated in Figure 15 (left) there was a gap in the tail of Gutenberg-Richter distribution which confirms the prediction of the larger event. Following the event with magnitude ML1.5, the gap is filled and the b-value changed slightly from 0.85 to 0.81 (Figure 15 right).

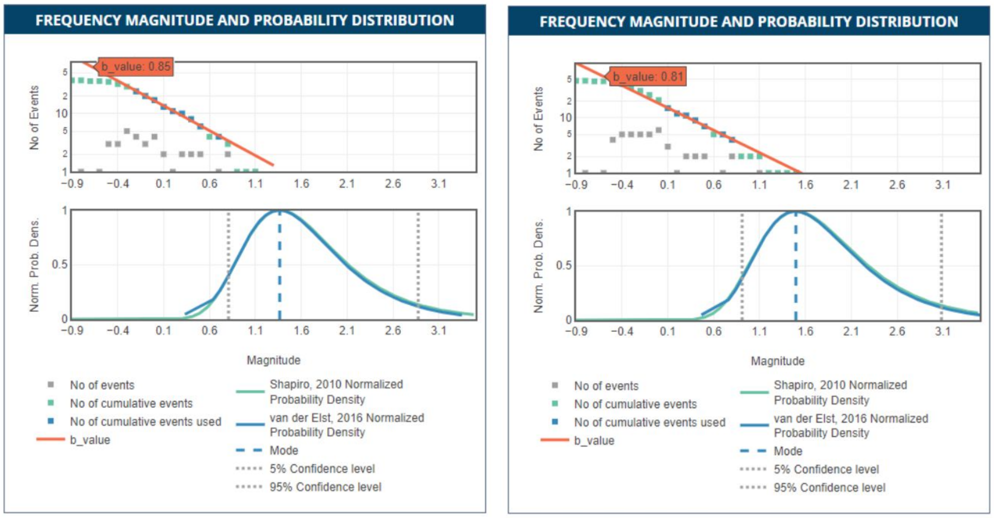

Figure 15: Gutenberg-Richter distribution and the normalised probability density function from SH10 (green line) and VDE16$_{Seis}$ (blue line) for the surface catalog (Left) before (Right) after the event with magnitude ML1.5

Combination of surface and downhole data

The larger events in the downhole catalog suffer from clipping and saturation due to the use of 15 Hz geophones, thereby we investigate the relationship between moment and local magnitude to combine the downhole and surface catalogs and generate a uniform catalog for further analysis.

Based on the origin time of events listed in the surface catalog, the common events in the downhole catalog were found. Figure 16 (left) illustrates the moment magnitude from downhole catalog versus the local magnitude from the surface catalog for the mutual events. We remove the events with differences in origin time larger than 0.75 seconds and also events with magnitude larger than ML0.6 (Figure 16 right). Following removal of outliers and underestimated magnitudes, the relationship between Mw and ML defined as:

$$Mw = 0.5262\ ML + 0.2513 \qquad (2)$$

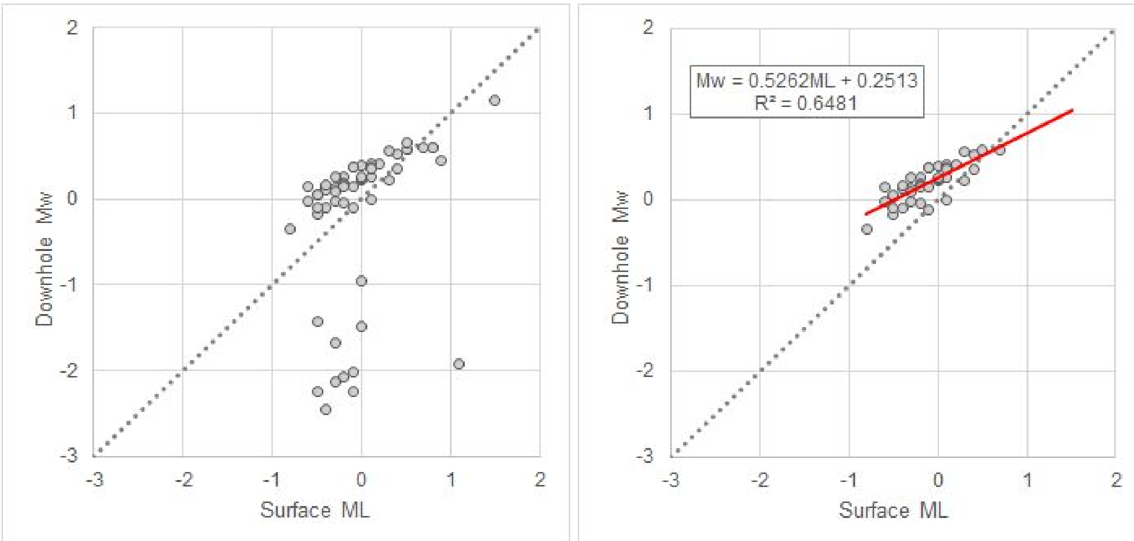

Figure 16: (Left) Moment magnitude from downhole catalog versus the local magnitude from the surface catalog for common events (right) Regression relationship between Mw and ML following outlier removal (red line). The gray dotted line denotes 1:1 line

In addition to developing Mw-ML conversion relationship, we investigate the applicable published models. Munafo et al. 2016 defined a general relationship (equation 3) that is globally valid up to Mw4, in which the constant C' only depends on the characteristics of the crustal attenuation of the study region that needs to be locally calibrated:

$$Mw = 2/3\ ML + C' \qquad (3)$$

Using the Alto Tiberina fault in the Upper Tiber valley of the northern Apennines of Italy, Munafo et al. 2016 defined C’ = 1.15. In the EPP Manager, 2019 report this relationship was modified by considering C’ = 0.9 as follow:

Figure 17 (top-left) displays the moment magnitude from downhole catalog as a function of converted surface moment magnitude using equation 3 considering C’ = 1.15. The trend of the data points follows 1:1 line, however, there is an offset which shows that the original equation with C’ = 1.15 does not fit the data. Examining equation 3 with C’ = 0.9 also does not fit the Preston New Road 2018 dataset (Figure 17 top-right).

In this study, we modify the constant coefficient to C’ = 0.2 and find a good fit to the data (Figure 17 bottom-left).

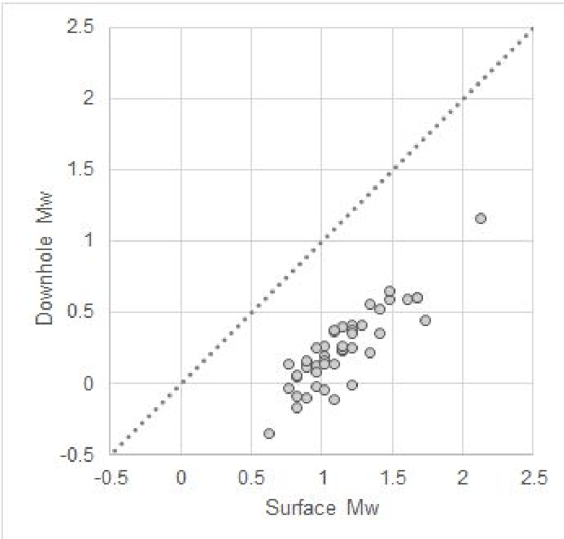

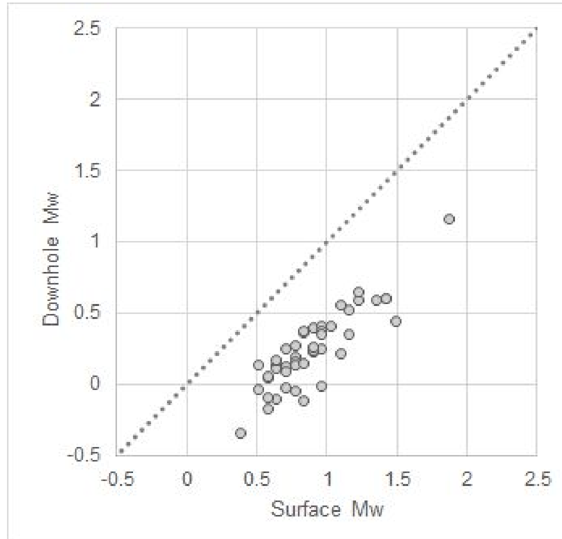

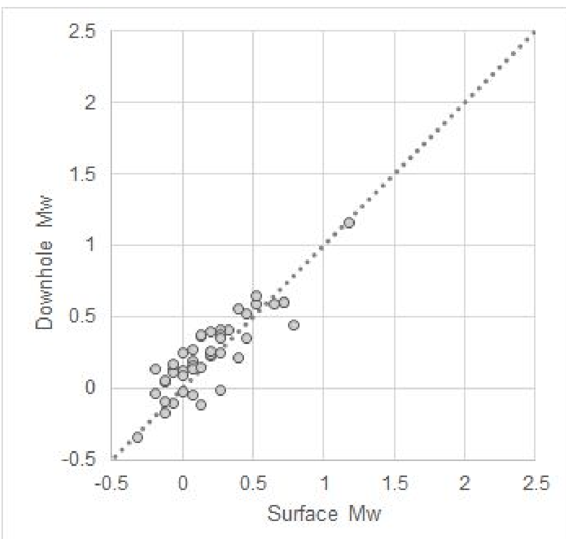

Figure 17: Moment magnitude from downhole catalog versus converted moment magnitude from surface acquisition using original model from Munafo et al. 2016 (Top-left) with C' = 1.15 (Top-right) with C' = 0.9 (Bottom-left) proposed C' = 0.2. The gray dotted line denotes 1:1 line

Figure 18 presents a side by side comparison of the two models which fit the data well. The figure on the left is showing the data using equation 2 and the image on the right displays the data using the Munafo et al. 2016 model with C' = 0.2.

The downhole 15 Hz geophones clipped for the largest event with a magnitude of Mw1.15. By using equation 3 with C'=1.15, the moment magnitude for this event is estimated as Mw1.05 which is smaller than the Mw1.15. This shows that this equation does not properly convert the local magnitude to moment magnitude (Figure 18 left). Using C'=0.9 results in Mw1.18 which is slightly larger than recorded downhole magnitude.

Following this analysis, the Munafo et al. 2016 model with C' = 0.2 was used to reevaluate the magnitude of eight common stronger events with reported downhole magnitude larger than Mw0.5. The updated uniform catalog was the new input into the forecasting seismicity analysis.

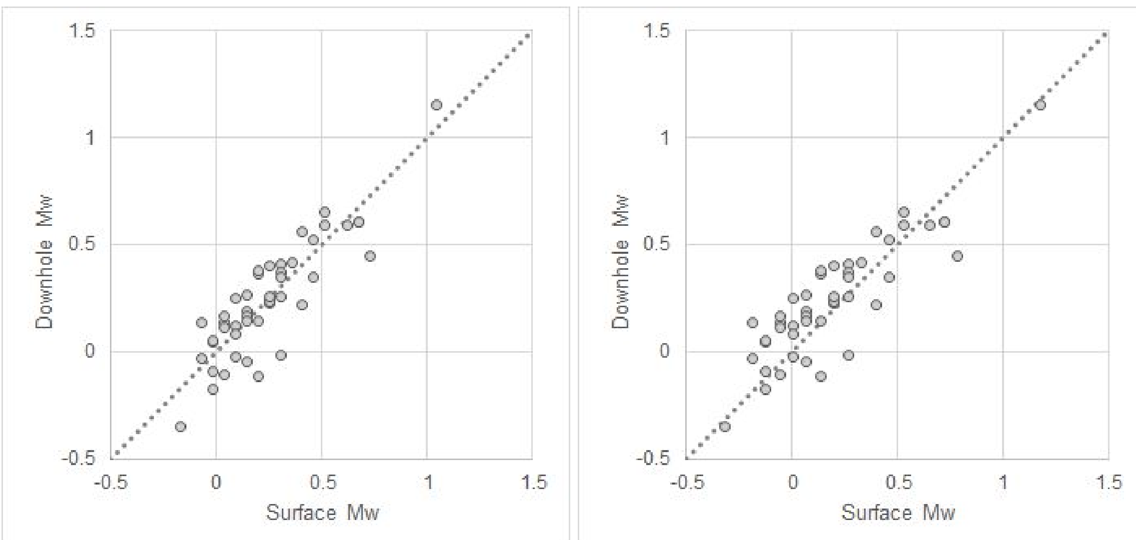

Figure 18: Moment magnitude from downhole catalog versus converted moment magnitude from surface data (Left) using Mw = 0.5262 ML + 0.2513 (Right) using Mw = 2/3 ML + 0.2. The gray dotted line denotes 1:1 line

The result from statistical analysis on the combined catalog is comparable to the result of the analysis using the entire downhole catalog (Figure 19). Five increasing steps of Mmax were observed during the monitoring time and the models successfully forecasted all of them with notification time varying from 1 to 16 days. Similar to the previous analysis H14 model overestimates the Mmax.

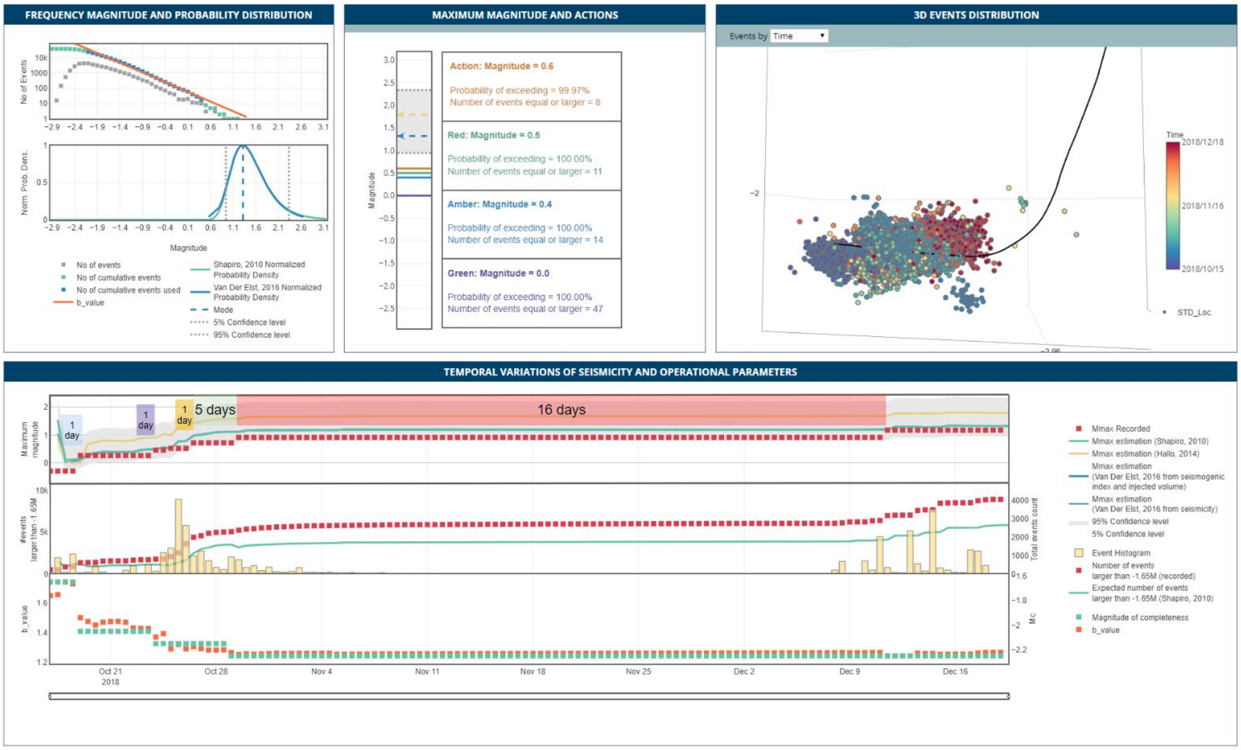

Figure 19: Dashboard for the combined surface and downhole uniformed catalog (see the caption of Figure 1 for descriptions of each panel)

Conclusions

In this study, we evaluate the performance of the forecasting models proposed by Shapiro et al. (2010), two models from Van Der Elst et al. (2016) and Hallo et al. (2014) for estimation of Mmax and number of events using the data recorded by the downhole and surface arrays during operation of Preston New Road (PNR) in 2018. The summary of our observations is as follows:

- The cumulative injection volume has low to no impact on forecasted seismicity, and over time, the forecasts lose sensitivity to the cumulative injection volume
- The estimated maximum magnitude from Shapiro et al. 2010 and Van Der Elst et al. 2016 models are very close in all test cases
- Hallo et al. 2014 model overestimates the maximum magnitude in many cases by ~0.5 magnitude units. We believe this is the result of adding 0.5 magnitude following Verdon and Budge (2018).
- Estimated maximum magnitudes from Shapiro et al. 2010 and Van Der Elst et al. 2016 models agree well with the observed largest magnitude for both entire downhole and surface catalogs
- The models successfully forecast all four larger events, using all downhole events
- Using the entire downhole data provides early forecasts of large magnitude events
- In this case study, forecasting was not very successful for data from individual stages. We believe the impact of injecting previous stages on the overall changes of the stress condition are disregarded by studying each stage separately.
- Combination of downhole and surface data is not impacting the results, as the updated magnitudes for the eight larger events are very close to the original moment magnitudes listed in the downhole catalog.

References

Bao, X., and D.W. Eaton, 2016, Fault activation by hydraulic fracturing in Western Canada, Science, DOI: 10.1126/science.aag2583.

Eaton, D. W. and N. Igonin, 2018, What controls the maximum magnitude of injection-induced earthquakes?" The Leading Edge, 37(2), 135–140, Doi.org/10.1190/tle37020135.1.

Geophysicist, EPP Manager, 2019, Hydraulic Fracture Plan PNR 2, Appendix 6: Ground Motion Prediction Equation (GMPE), Cuadrilla Resources Ltd

Hallo, M. I. Oprsal, L. Eisner, and M. Y. Ali, 2014, Prediction of magnitude of the largest potentially induced seismic event, J. Seismol. 18, 421–431.

Kiraly-Proag, E., J. D. Zechar, V. Gischig, S. Wiemer, D. Karvounis, and J. Doetsch, 2016, Validating induced seismicity forecast models - Induced Seismicity Test Bench, Journal of Geophysical Research. Solid Earth, 121, 6009–6029. https://doi.org/10.1002/2016JB013236

Munafò, I. Malagnini, L and L. Chiaraluce, 2016, On the Relationship between Mw and ML for Small Earthquakes, Bulletin of the Seismological Society of America, Vol. 106, No. 5, pp. 2402–2408, doi: 10.1785/0120160130

McGarr, A., 2014, Maximum magnitude earthquakes induced by fluid injection: Journal of Geophysical Research. Solid Earth, 119, no. 2, 1008–1019, https://doi.org/10.1002/2013JB010597.

Schultz1, R. Atkinson, G. Eaton, D. W. Gu, Y. J. and H. Kao, 2018, Hydraulic fracturing volume is associated with induced earthquake productivity in the Duvernay play, Science, DOI: 10.1126/science.aao0159.

Shapiro, S. A., C. Dinske, C. Langenbruch, and F. Wenzel, 2010, Seismogenic index and magnitude probability of earthquakes induced during reservoir fluid stimulations: The Leading Edge, 29, no. 3, 304–309, https://doi.org/10.1190/1.3353727.

Shapiro, S. A., Krüger, O. S. Dinske, C. and C. Langenbruch, 2011, Magnitudes of induced earthquakes and geometric scales of fluid-stimulated rock volumes: Geophysics, 76, no. 6, WC55–WC63, https://doi.org/10.1190/geo2010-0349.1.

250 Herzberg Road, Kanata, Ontario, Canada K2K 2A1
Tel +1 613 592 6776 | **Toll Free** 1 855 792 6776 (NA) | **Fax** +1 613 592 5929

Van der Elst, N. J., Page, M. T. Weiser, D. A. Goebel, T. H. W. and S. M. Hosseini, 2016, Induced earthquake magnitudes are as large as (statistically) expected: Journal of Geophysical Research. Solid Earth, 121, no. 6, 4575–4590, https://doi.org/10.1002/2016JB012818.

Verdon, J. P., and J. Budge, 2018, Examining the capability of statistical models to mitigate induced seismicity during hydraulic fracturing of shale gas reservoirs, Bull. Seismol. Soc. Am. 108, 690–701.

Contact information

Sepideh Karimi PhD.

Research Scientist Lead

P: +1 613 505 5121

sepidehkarimi@nanometrics.ca

William Parrales P. Eng.

Senior Sales Manager

P: +1 403 444 5747

M: +1 403 680 9222

williamparrales@nanometrics.ca

Appendix A

In this section all the figures presented in the report are displayed in full size.

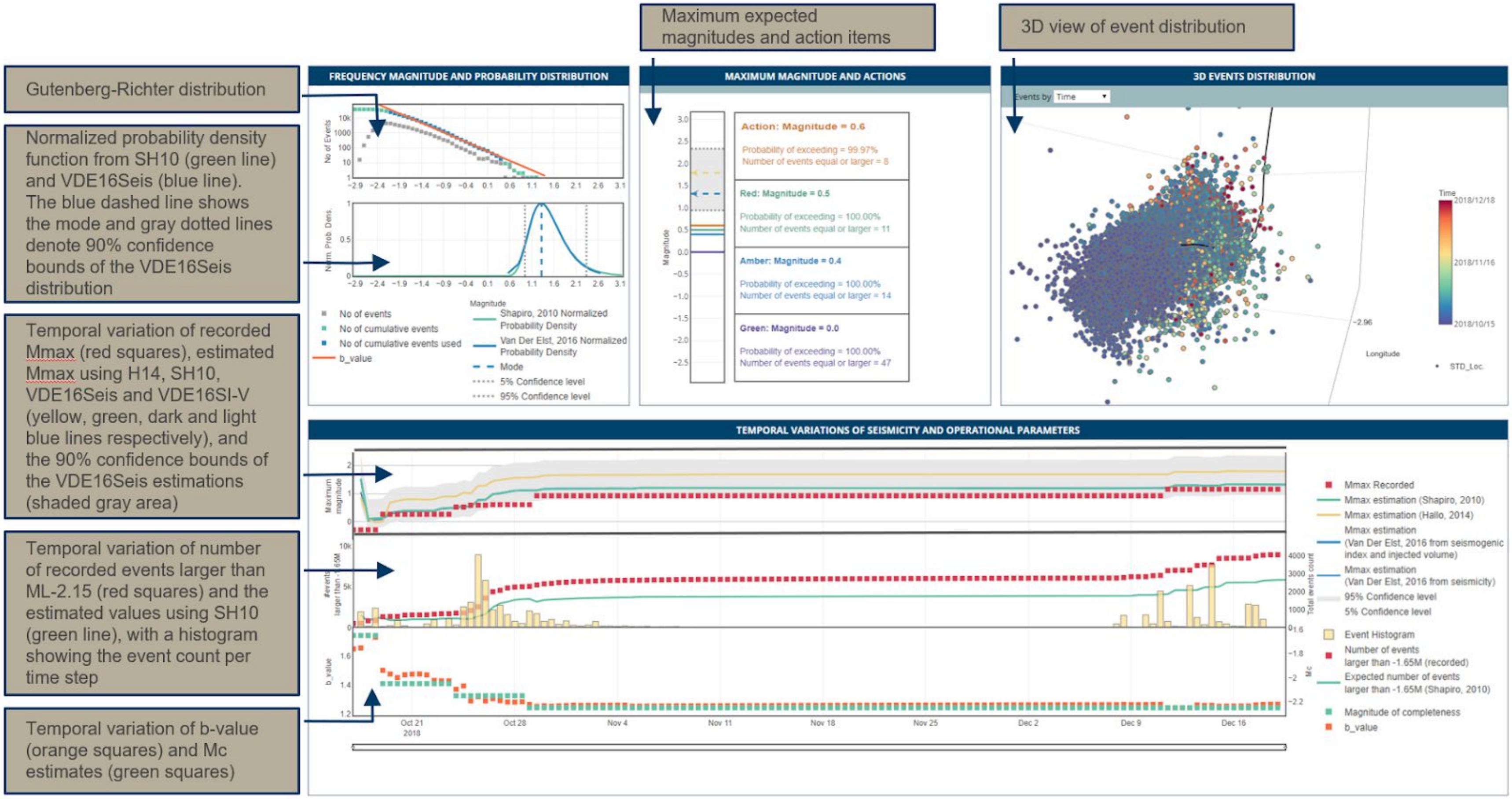

Figure 1: Example Nanometrics Seismic Management Dashboard with a description of each panel

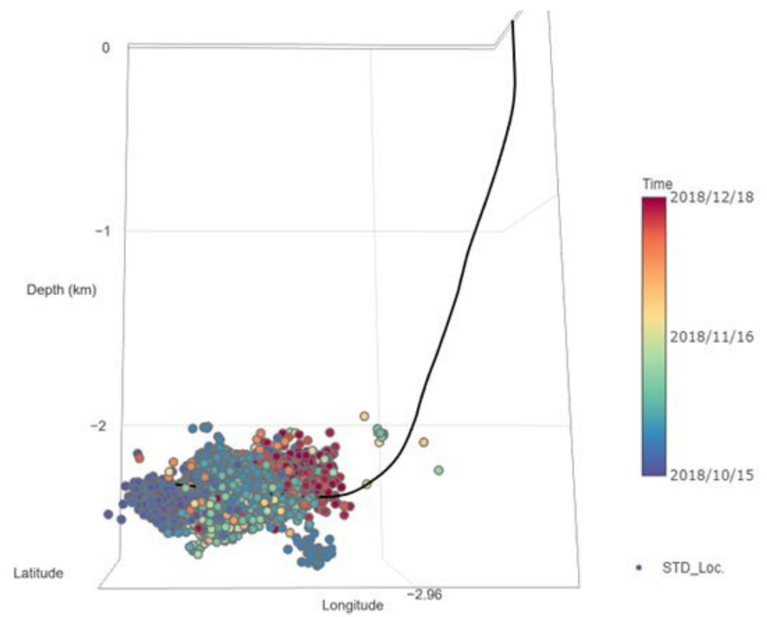

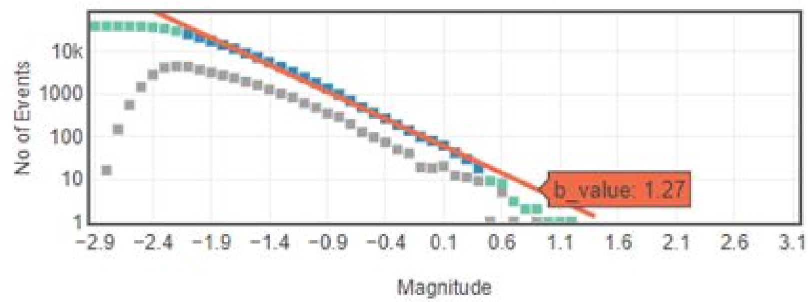

Figure 2: (Left) 3D distribution of the recorded seismicity by the downhole monitoring array (Top) Gutenberg-Richter distribution for the entire catalog with b-value of 1.27

250 Herzberg Road, Kanata, Ontario, Canada K2K 2A1

Tel +1 613 592 6776 | **Toll Free** 1 855 792 6776 (NA) | **Fax** +1 613 592 5929

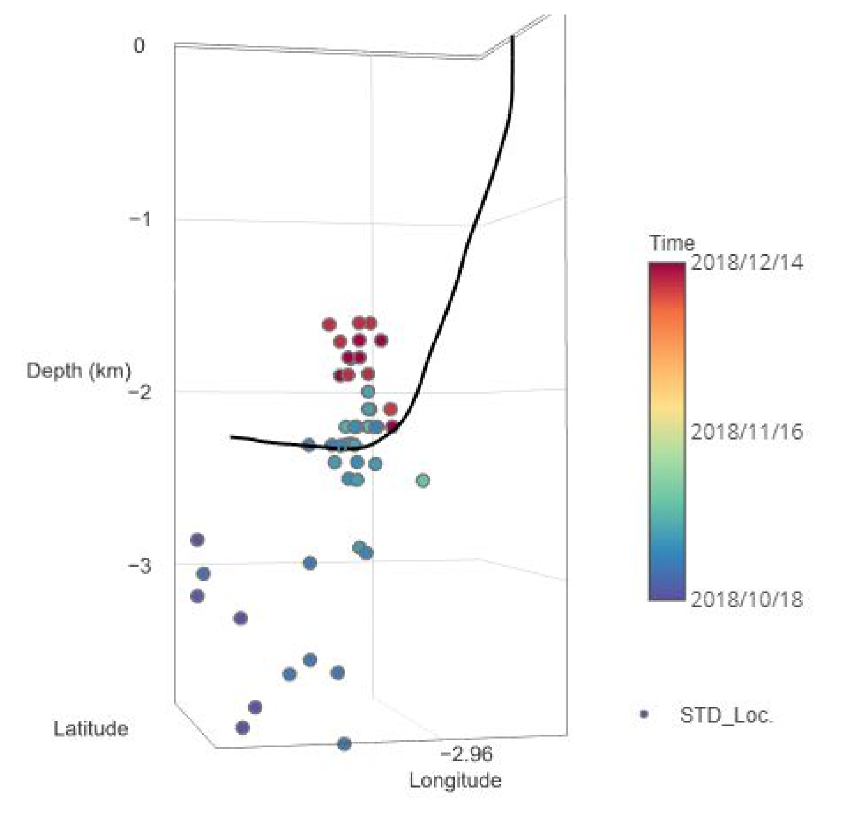

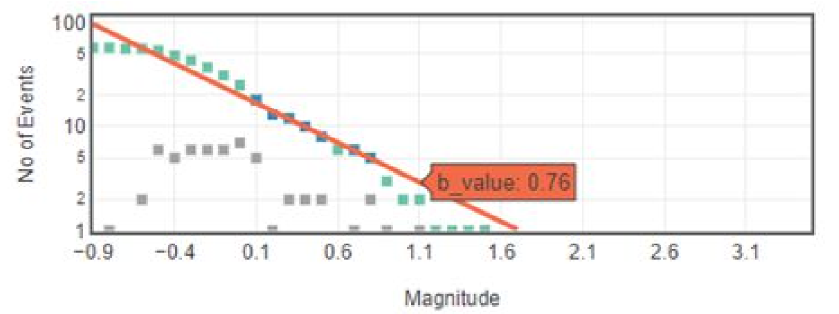

Figure 3: (Left) 3D distribution of the recorded seismicity by the surface array (Top) Gutenberg-Richter distribution for the entire catalog with b-value of 0.76

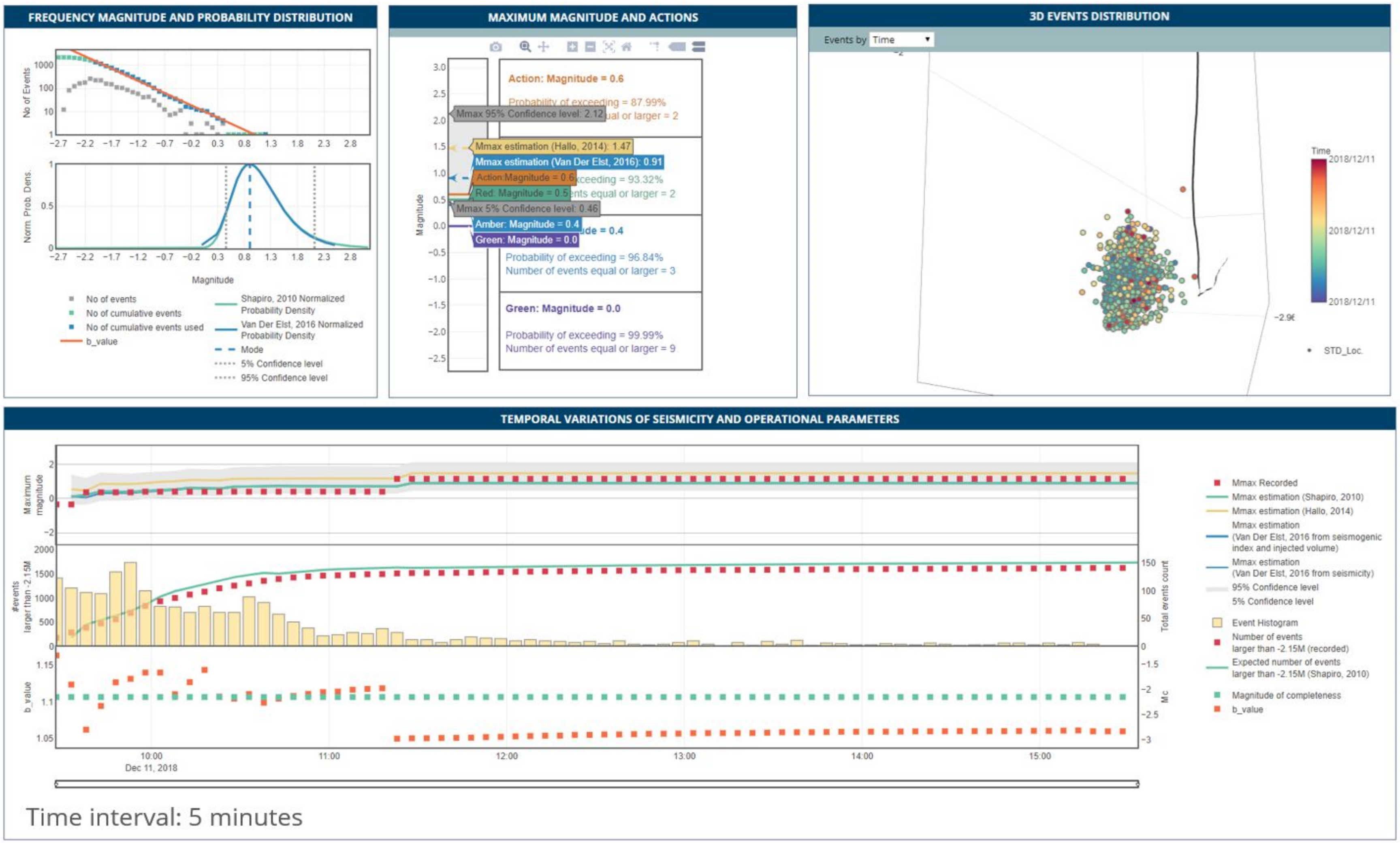

Figure 4: Dashboard for recorded seismicity by the downhole array during stimulation on sleeve 38 using real cumulative injection volume

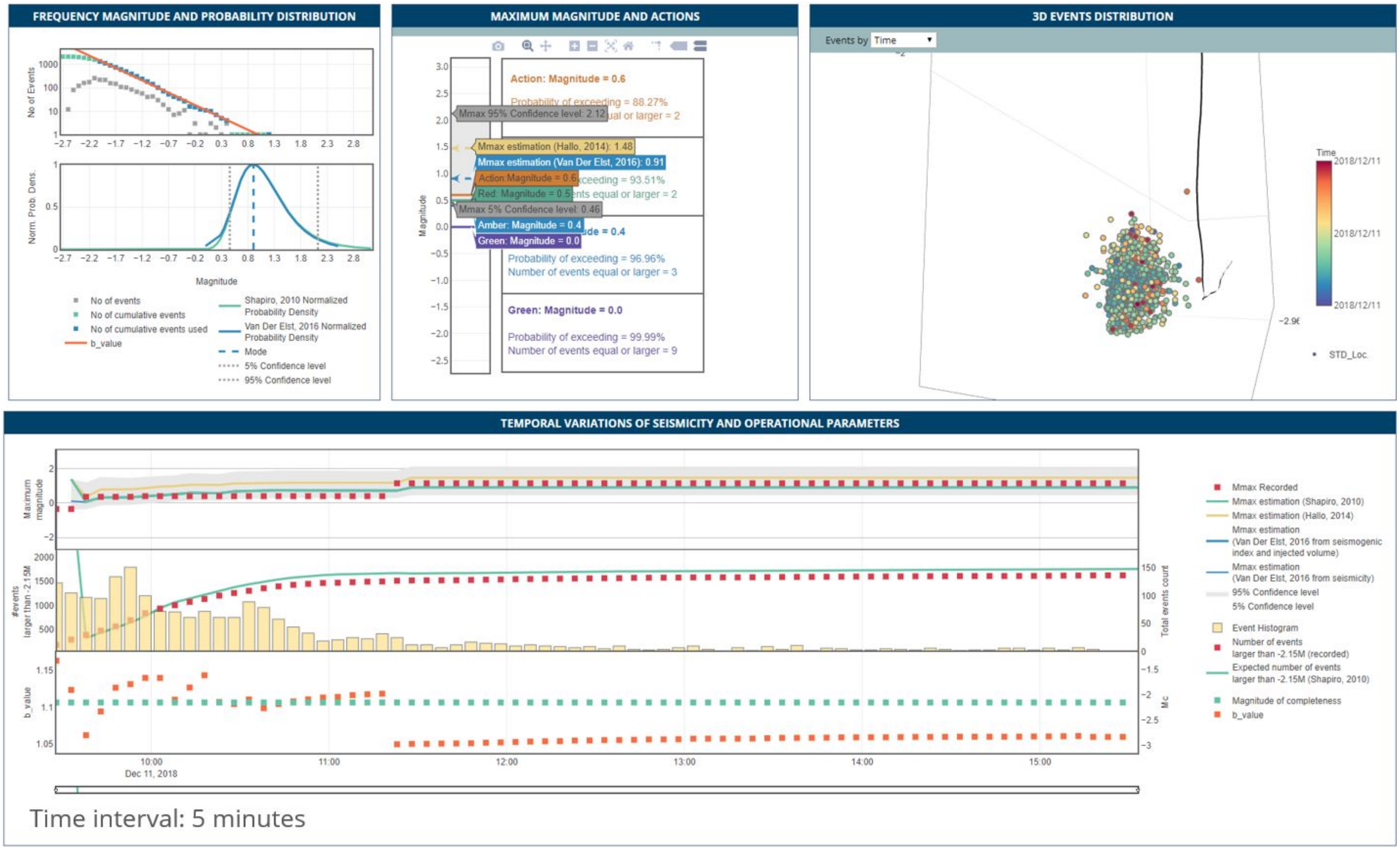

Figure 5: Dashboard for recorded seismicity by the downhole array during stimulation of sleeve 38 using simulated cumulative injection volume with a steady increasing rate (see the caption of Figure 1 for descriptions of each panel)

250 Herzberg Road, Kanata, Ontario, Canada K2K 2A1

Tel +1 613 592 6776 | **Toll Free** 1 855 792 6776 (NA) | **Fax** +1 613 592 5929

Figure 6: Dashboard for recorded seismicity by the downhole array during stimulation of sleeve 14, with observed Mmax of Mw0.52 (see the caption of Figure 1 for descriptions of each panel)

Figure 7: Dashboard for recorded seismicity by the downhole array during stimulation of sleeve 18, with observed Mmax of Mw0.59 (see the caption of Figure 1 for descriptions of each panel)

Figure 8: Dashboard for recorded seismicity by the downhole array during stimulation of sleeve 30, with observed Mmax of Mw0.61 (see the caption of Figure 1 for descriptions of each panel)

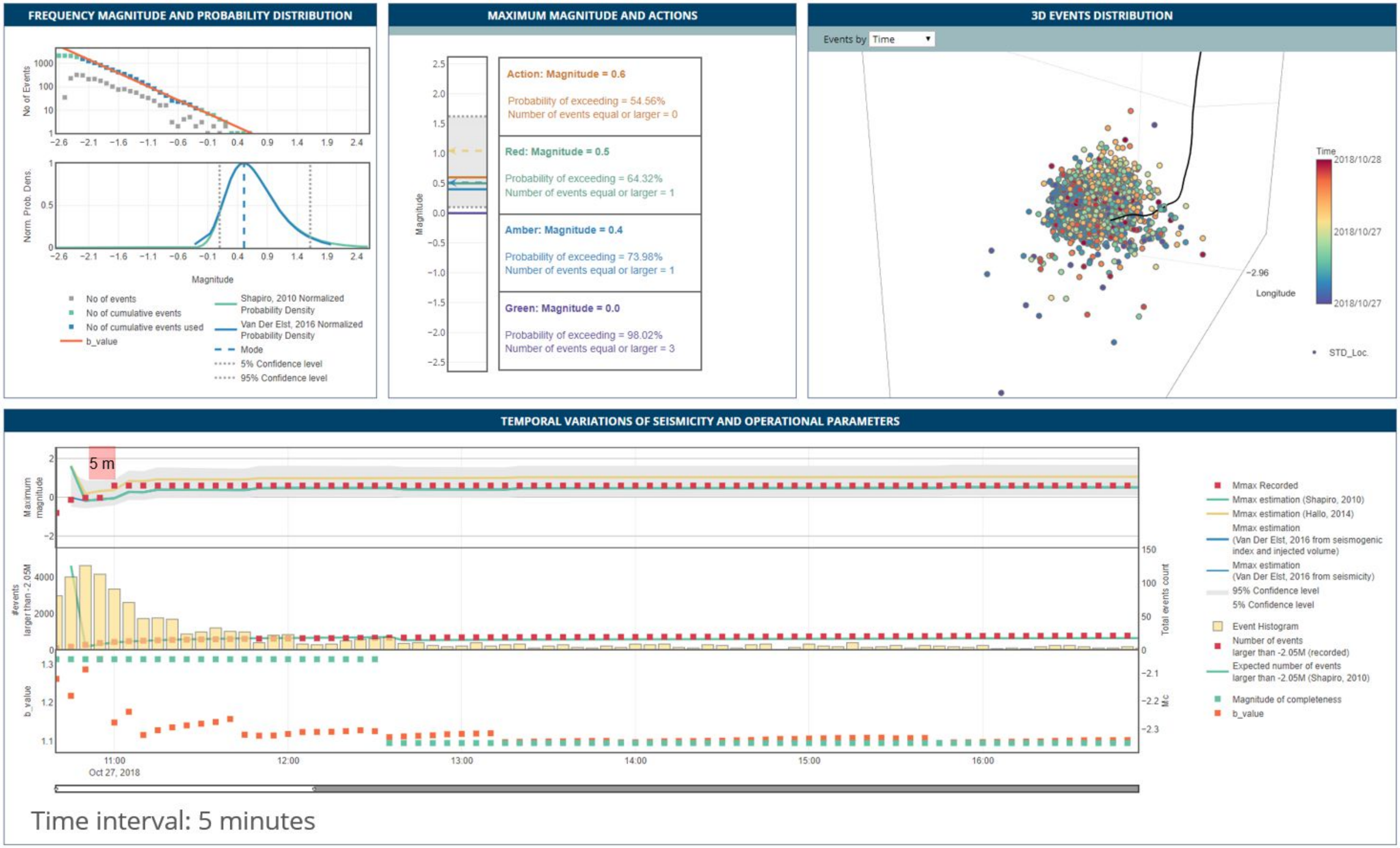

Figure 9: Dashboard for recorded seismicity by the downhole array during stimulation of sleeve 31 with observed Mmax of Mw0.61 (see the caption of Figure 1 for descriptions of each panel)

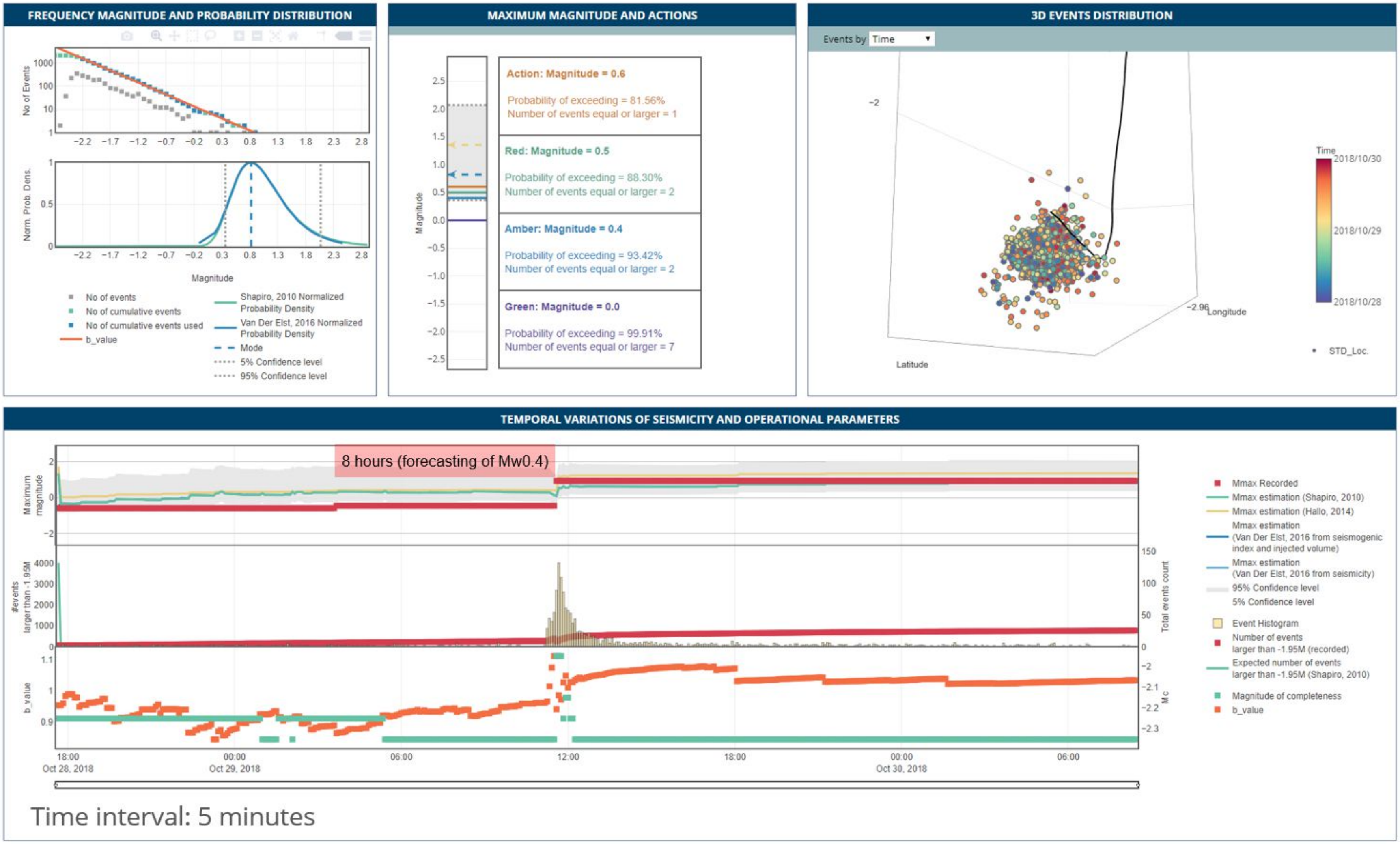

Figure 10: Dashboard for recorded seismicity by the downhole array during stimulation of sleeve 32, with observed Mmax of Mw0.93 (see the caption of Figure 1 for descriptions of each panel)

Figure 11: Dashboard for recorded seismicity by the downhole array during stimulation of sleeve 35, with observed Mmax of Mw0.59 (see the caption of Figure 1 for descriptions of each panel)

Figure 12: Dashboard for recorded seismicity by the downhole array during stimulation of sleeve 38, with observed Mmax of Mw1.15 (see the caption of Figure 1 for descriptions of each panel)

Figure 13: Dashboard for the entire recorded seismicity by the downhole array. The forecasting notification time is highlighted. (see the caption of Figure 1 for descriptions of each panel)

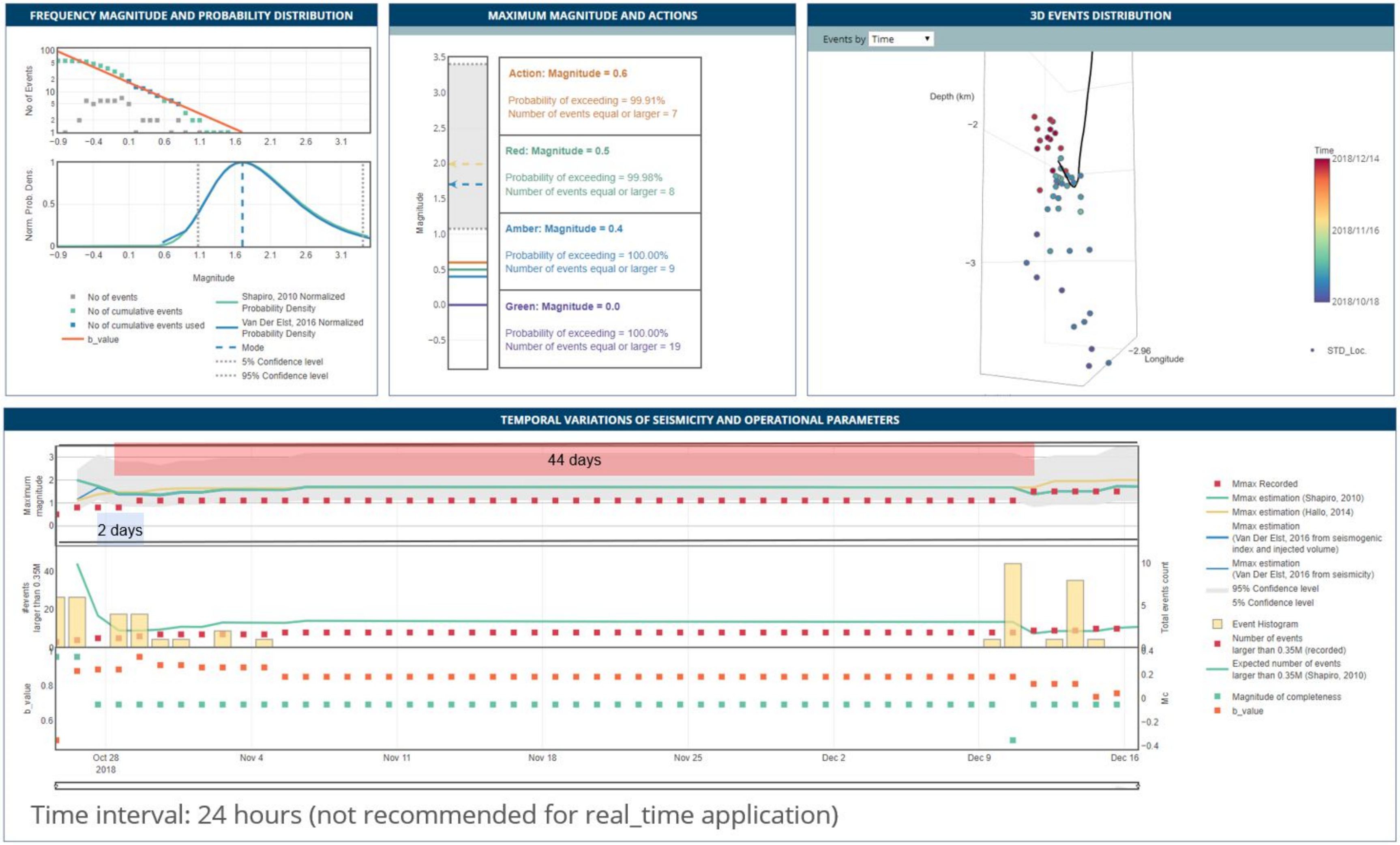

Figure 14: Dashboard for the entire recorded seismicity by the surface array (see the caption of Figure 1 for descriptions of each panel)

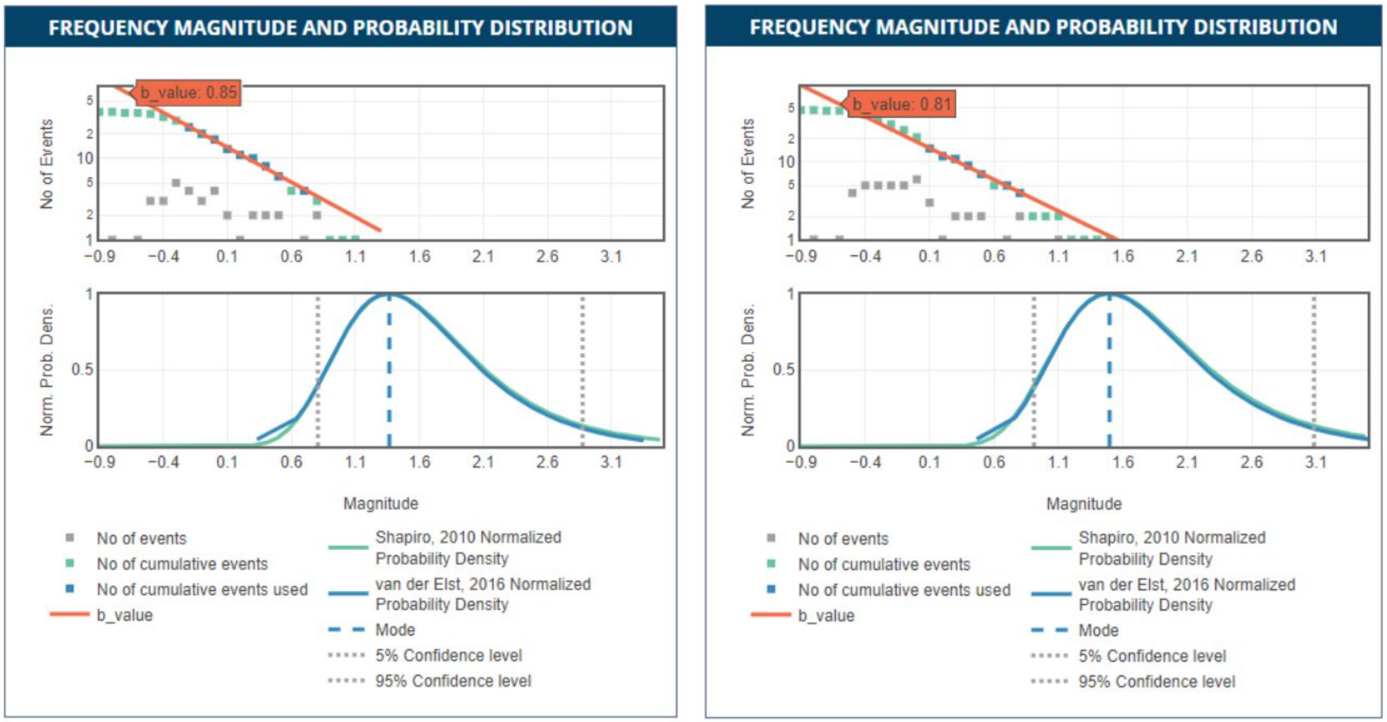

Figure 15: Gutenberg-Richter distribution and the normalised probability density function from SH10 (green line) and VDE16$_{Seis}$ (blue line) for the surface catalog (Left) before (Right) after the event with magnitude ML1.5

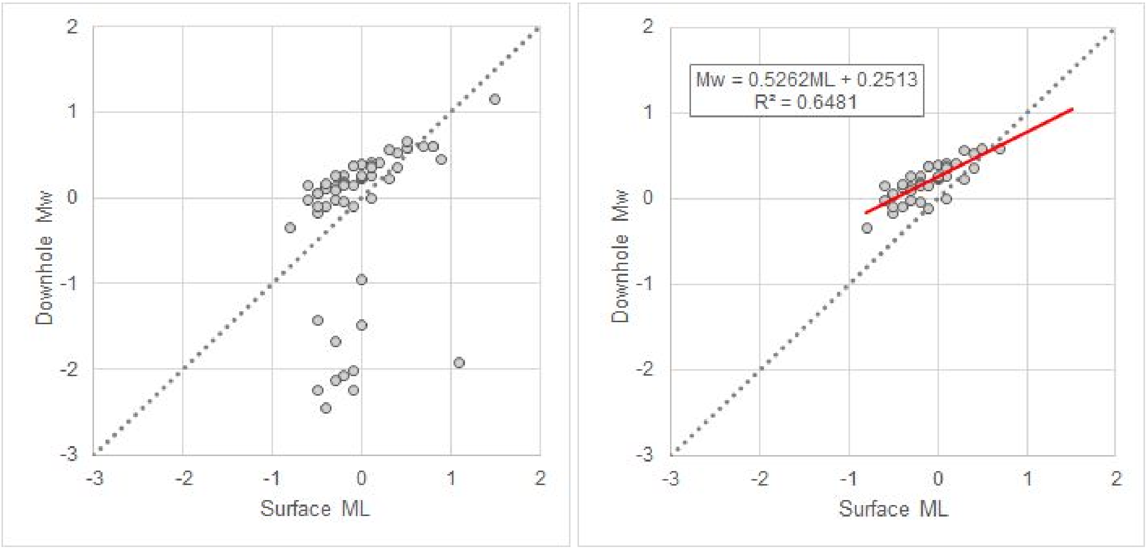

Figure 16: (Left) Moment magnitude from downhole catalog versus the local magnitude from the surface catalog for common events (right) Regression relationship between Mw and ML following outlier removal (red line). The gray dotted line denotes 1:1 line

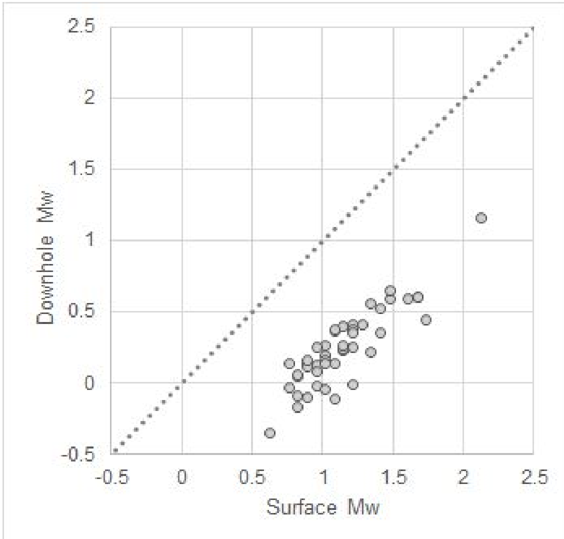

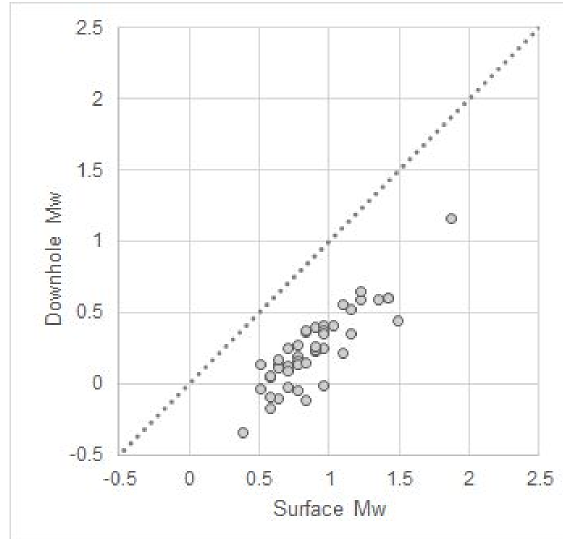

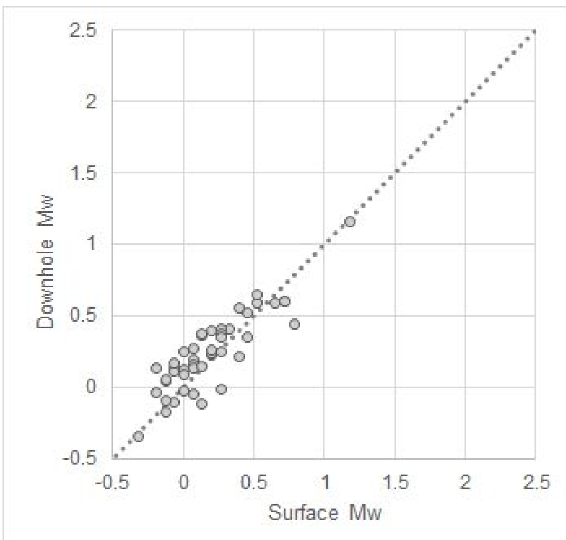

Figure 17: Moment magnitude from downhole catalog versus converted moment magnitude from surface acquisition using original model from Munafo et al. 2016 (Top-left) with C′ = 1.15 (Top-right) with C′ = 0.9 (Bottom-left) proposed C′ = 0.2. The gray dotted line denotes 1:1 line

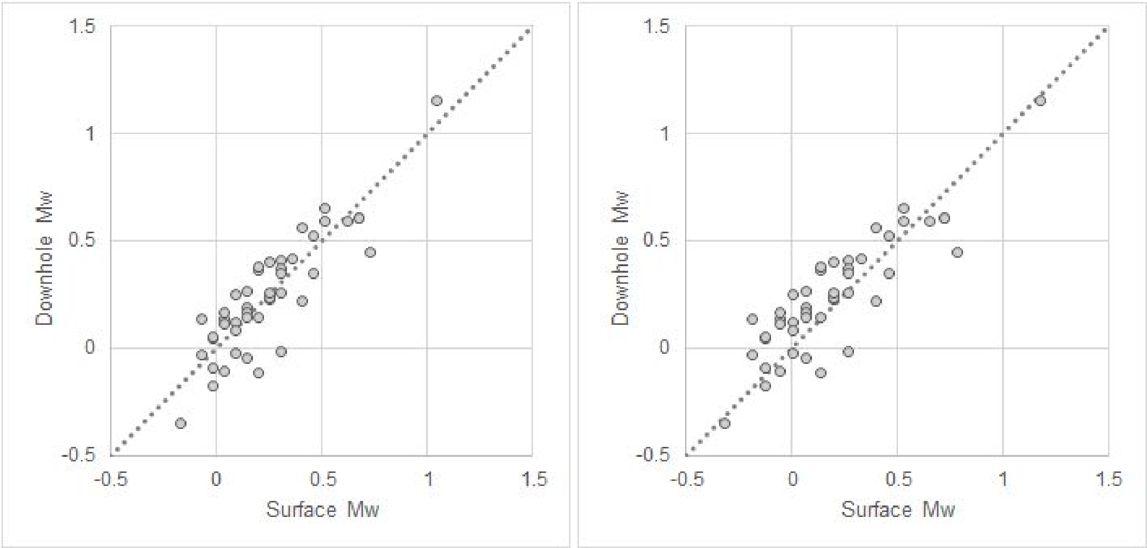

Figure 18: Moment magnitude from downhole catalog versus converted moment magnitude from surface data (Left) using Mw = 0.5262 ML + 0.2513 (Right) using Mw = 2/3 ML + 0.2. The gray dotted line denotes 1:1 line

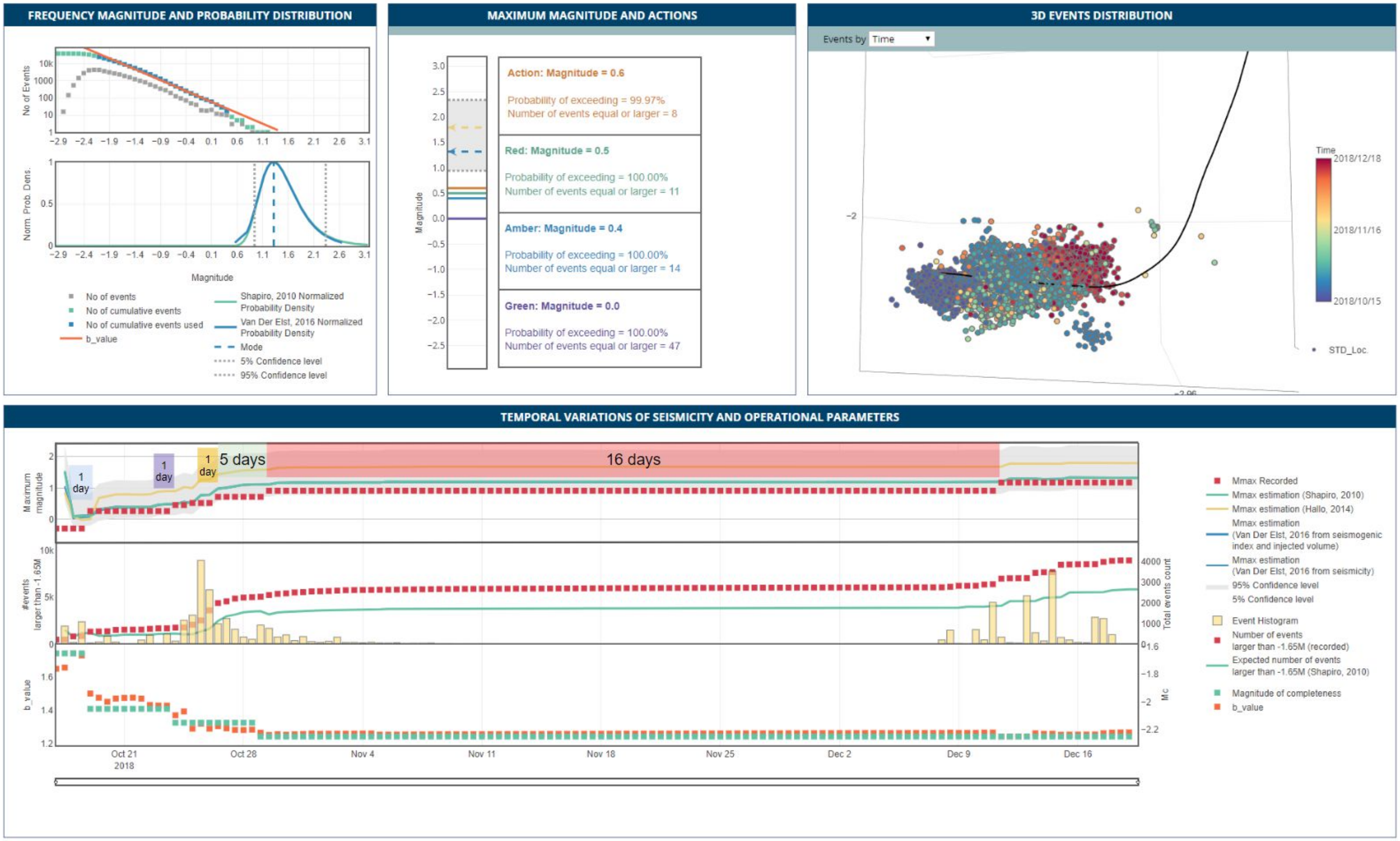

Figure 19: Dashboard for the combined surface and downhole uniformed catalog (see the caption of Figure 1 for descriptions of each panel)

Appendix B

The seismicity forecasting models used in this study are from:

- Shapiro et al. (2010) equations 3, 4 and 5 in the original paper
- Hallo et al. (2014) equations 5 and 6 in the original paper
- Van Der Elst et al. (2016) equations 1, 2 and 4 in the original paper

250 Herzberg Road, Kanata, Ontario, Canada K2K 2A1
Tel +1 613 592 6776 | **Toll Free** 1 855 792 6776 (NA) | **Fax** +1 613 592 5929